Waveform of gravity and capillary-gravity waves over a bathymetry

Jie Yu*

Naval Research Laboratory, Stennis Space Center, Mississippi 39529, USA

(Received 27 September 2018; published 22 January 2019)

We examine the waveforms of linear waves over a fully submerged, arbitrarily periodic bed, using the recent Floquet theory for gravity waves and extending it to the regime of capillary-gravity waves. The exact solutions illustrate the complex features of waveform geometry that are frequency dependent, including the modulation of propagating waveforms in space-time, spatially modulated standing waveforms, asymmetric waveforms over a symmetric bed profile, and high-curvature wave-crest forms. These features are in contrast to the trivial and invariant sinusoidal waveform of the ordinary linear waves on a flat bed, but reminiscent of nonlinear waveforms. The effect of surface tension is seen to counteract wave scattering by topography, tending to restore the waveform towards a symmetric and sinusoidal geometry. These features are the general characteristics of linear waves over a periodic bed since they are the properties of eigenmodes, and can inspire and guide applications.

DOI: 10.1103/PhysRevFluids.4.014806

I. INTRODUCTION

For two-dimensional time-harmonic motions over a horizontal flat bed, the classical Sturm-Liouville eigenvalue problem in the vertical z direction gives a complete basis of linear modes: For any frequency ω, there are two oppositely directed propagating waves of wave-number vectors $\pm k$, respectively. The wave number (eigenvalue) k satisfies the well-known dispersion relationship $\omega^2 = gk\tanh(kh)$, where h is the water depth and g is the gravitational acceleration. Correspondingly, the eigenfunctions are proportional to $e^{\pm ikx}\cosh k(z+h)$, respectively. For that same frequency ω, there are also two infinite families of evanescent modes that are identified by the eigenvalues $\pm\kappa_n$, where $\omega^2 = -g\kappa_n\tan(\kappa_n h)$, $n = 1, 2, \ldots$. Correspondingly, the eigenfunctions are proportional to $e^{\pm\kappa_n x}\cos\kappa_n(z+h)$, respectively. The amplitudes of these evanescent modes rapidly decay (or grow) in x, since $(n-1/2)\pi < \kappa_n h < n\pi$ hence is in general large. Until recently, this set of flat-bottom propagating and evanescent waves was the only known complete basis of linear modes for water waves and has played important roles in various problems involving lateral boundary conditions in the x direction, e.g., in engineering problems of floating body dynamics and wave-structure interactions [1]. It also has a significant place in numerical modeling of water waves. For instance, for rapidly varying topographies, one approach is to discretize the bottom into small pieces of horizontal steps, on each of which the solution is represented as a linear combination of these flat-bottom waves and evanescent modes appropriate to the local depth (see, e.g., Ref. [2] and references therein).

For an arbitrarily periodic bed, without any constraint on the undulation amplitude and shape but being fully submerged in a mean constant water depth, the studies in Refs. [3–5] have provided an approach that can be considered as a definitive solution to this type of problem. By constructing a conformal map and invoking the Floquet theory, the eigenvalue problem in the vertical direction

*Jie.Yu@nrlssc.navy.mil

(which is no longer the ordinary type of Sturm-Liouville eigenvalue problem as in the flat-bottom case) becomes tractable. The exact Floquet solutions given in [5] consist of a family of two wave modes and two infinite families of evanescent modes, analogous to the set of flat-bottom modes. This has become the second complete basis for water waves and can indeed be used, in a manner similar to the use of the flat-bottom basis, to solve a class of linear problems involving a periodic bed in confined or closed domains. Such applications (particular problems) include, for example, Bragg scattering by a patch of bottom corrugations confined between two flat beds [6] and resonant standing waves in a closed basin with a corrugated bottom [3,7].

While the evanescent modes are needed in practical problems to deal with the lateral boundary conditions in the x direction, it is the wave modes that are manifested away from boundaries. Since their focus was to construct the exact solutions on an arbitrarily periodic bed, Yu and Howard [5] did little to explore the waveforms (eigenfunctions), but classified the wave modes on the frequency domain based on the eigenvalues. The present study intends to fill this gap, i.e., to elucidate the physical phenomena that are obscured by the mathematical complexity of the solutions. As we will see, in contrast to a flat-bottom linear wave whose waveform is trivial, being sinusoidal regardless of the frequency and invariant in space-time as the wave propagates, the linear waveforms on a periodic bed are spatially complex and frequency dependent. While their nonsinusoidal geometry may be readily anticipated, some features are far from obvious and intriguing: The waveforms are spatially modulating when the wavelengths (the horizontal distance between two adjacent wave crests or troughs) are not an integer multiple of the topography period. The waveforms can be asymmetric with respect to wave crest (or trough) even though the bed profile is symmetric in x. Furthermore, the waveforms are not permanent, continuously changing their shapes as the waves propagate. These features are almost never associated with linear time-harmonic waves on a flat bed, but typically arise from nonlinear effects. These above mentioned features are the general characteristics of linear waves over a periodic bed, since they are the properties of eigenmodes. Moreover, since these features arise from the nonuniformity of surface oscillation that is caused by the variability in topography (see Sec. IV), it is reasonable to expect that some of them may similarly occur in the case of a nonperiodic bed. Since linear solutions are often applied in practical problems and are the first step in many nonlinear analyses, the results of this study will contribute to the literature and guide applications.

To have a complete study of the waveforms over a periodic bed, we will first extend the exact theory of [5] to the regime of capillary-gravity waves, since this class of waves can feel the changes in the water depth and hence be affected by the bed variations. For linear capillary-gravity waves on a flat bed, the dispersion relationship is well known, i.e.,

$$\omega^2 = gk \tanh(kh)[1 + Tk^2/\rho g], \tag{1}$$

where T is the surface tension and ρ is the fluid density. In the limit of an infinite depth, a critical wave number $k_c = \sqrt{\rho g/T}$ can be identified where the wave speed is minimal [8]. The critical wavelength $\lambda_c = 2\pi/k_c$ is a reference length separating the regimes of capillary waves ($g = 0$) and gravity waves ($T = 0$). For finite depths, such a minimum wave speed does not exist when the depth is sufficiently shallow ($k_c h < \sqrt{3}$). Nevertheless, in the vicinity of λ_c the dispersion relationship of a capillary-gravity wave is significantly different from that of a capillary wave or a gravity wave (see Fig. 1). Because of the triviality of linear waveforms on a flat bed, research interests have been mostly directed to nonlinear capillary-gravity waves (see the reviews in Refs. [9,10] and the references therein). While many studies in the literature focus on the case of infinite fluid depth, there does exist interest in cases of finite depths (e.g., Refs. [9,11–13]). However, there has been little effort to address the effect of a variable bed on capillary-gravity waves.

For gravity waves, we have known that strong topographic scattering occurs when the surface wavelength λ is comparable to the bed period λ_b. In view of Fig. 1, we expect that the effects of bed topography and surface tension on surface waves are comparable when λ, λ_b, λ_c, and the fluid depth are of similar magnitude. In oscillatory flows, the effect of viscosity typically is confined within the Stokes boundary layer of thickness proportional to $\sqrt{2\nu/\omega}$ (for Newtonian fluids), where ν is the

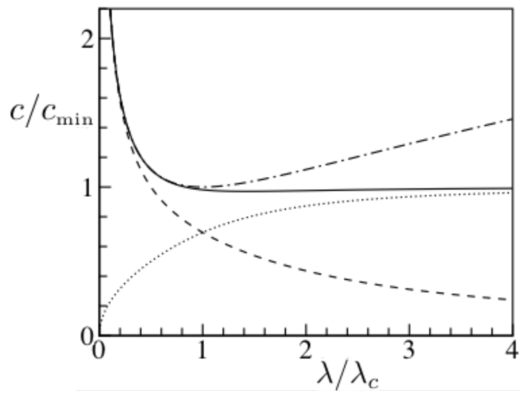

FIG. 1. Dispersion relationship for water waves on a flat bed. For $k_c d = 2.0$: ——, a capillary-gravity wave; – – –, a capillary wave ($g = 0$); $\cdots\cdots$, a gravity wave ($T = 0$). For deep water ($k_c d \gg 1$): – · – · –, a capillary-gravity wave. The critical wave speed $c_{\min} = \sqrt{2g/k_c}$.

fluid viscosity. For high frequencies that are appropriate for capillary-gravity waves, this viscous layer can be very thin. For example, for water $\lambda_c = 17.12$ mm, but the Stokes layer thickness is of 0.18 mm or thinner for a frequency of 10 Hz or higher. Thus, we anticipate that the potential theory of capillary-gravity waves in this study can be useful in some small-scale applications where manipulations of periodic boundary geometry and oscillation frequencies are of interest.

The outline of the paper is as follows. In Sec. II we present the exact solutions for capillary-gravity waves over an arbitrarily periodic bed. To be self-contained and sufficiently clear, some mathematical details are included, despite their familiar appearance in the previous studies. Calculations of the dispersion relationship are shown in the Appendix, where the limiting case of a flat bed is included for verification. Bragg resonance bands (gaps) are shown for selected bed profiles in Sec. III. The frequencies inside these bands are forbidden for waves over a periodic bed of indefinite length, but of special interest in cases where the periodic bed is confined to a patch of finite length or enclosed in a domain. In Sec. IV we discuss the properties of gravity and capillary-gravity waveforms for the frequencies outside a resonance band and for the threshold frequencies at the boundaries of a band. The apparent similarities to nonlinear waveforms are explained. Concluding remarks are in Sec. V.

II. EXACT FLOQUET THEORY OF CAPILLARY-GRAVITY WAVES

Consider a layer of homogeneous fluid over a periodic seabed. Denoting the dimensional variables by the prime, in the vertical plane (x', z'), $z' = 0$ is the undisturbed free surface and the seabed is at $z' = -h'_0 + h'_b(x')$, where $h'_b(x')$ describes an arbitrarily periodic bed profile. The spatial period of h'_b is λ_b, which sets the intrinsic periodicity of the medium in which waves propagate. Without losing any generality, we will make $h'_b(x')$ have a zero average in x' so that h'_0 represents the mean undisturbed fluid depth. The bed elevation varies over a vertical range of $\Delta h'_b = h'_{b,\max} - h'_{b,\min}$, which is called the undulation height.

Let $\phi'(x', z', t')$ be the velocity potential and $\zeta'(x', t')$ be the surface elevation measured from $z' = 0$. We define a wave number

$$k_B = \pi/\lambda_b \tag{2}$$

that corresponds to a surface wavelength of $2\lambda_b$ and choose the normalization

$$x = k_B x', \quad z = k_B z', \quad t = t'\sqrt{gk_B}, \quad \phi = \phi'/(a\sqrt{gk_B}/k_B), \quad \zeta = \zeta'/a, \tag{3}$$

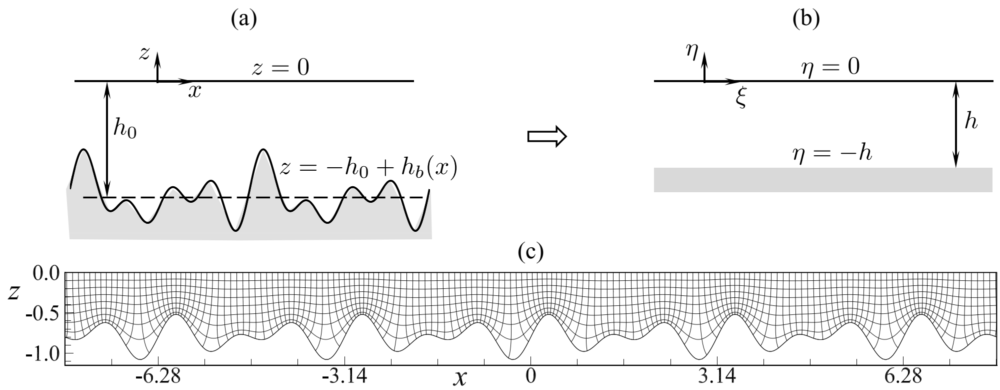

FIG. 2. (a) Sketch of a homogeneous fluid layer over a periodic bed for $-\infty < x < \infty$ and $-h_0 + h_b(x) \leqslant z \leqslant 0$. (b) Uniform strip of the flow domain upon conformal transformation for $-\infty < \xi < \infty$ and $-h \leqslant \eta \leqslant 0$. (c) Orthogonal curvilinear grids in the (x, z) plane that correspond to the Cartesian grids $\xi =$ const and $\eta =$ const, showing the terrain-following contours near the bottom.

where the surface amplitude a is arbitrarily small compared to the fluid depth and surface wavelength. The dimensionless bed profile $h_b(x) = k_B h'_b(x')$ is π periodic and the mean water depth $h_0 = k_B h'_0$. The linearized equations for ϕ are

$$\phi_{xx} + \phi_{zz} = 0 \quad \text{for } -h_0 + h_b(x) < z < 0, \tag{4}$$

$$\phi_x h_{b,x} = \phi_z \quad \text{at } z = -h_0 + h_b(x), \tag{5}$$

$$\zeta_t = \phi_z \quad \text{at } z = 0, \tag{6}$$

$$\phi_t + \zeta - \kappa\zeta_{xx} = 0 \quad \text{at } z = 0, \tag{7}$$

where

$$\kappa = T k_B^2/\rho g \tag{8}$$

is the inverse of the Bond number based on the length λ_b/π and the t, x, and z subscripts denote partial derivatives. Note that $\kappa = (k_B/k_m)^2$ and hence compares the effects of surface tension and topographic scattering: A larger value of κ means that the capillary effect is more important than wave scattering by topography.

The scaling in Eq. (3) is most appropriate when λ_b/λ is small or finite. For sufficiently short waves, scattering by topography is ineffective since the waves would be either in deep-water conditions or locally on an approximately flat bed (if the water depth is very shallow). Whereas the exact Floquet theory still is valid in this case, it may be more efficient to treat the waves as in deep waters (or approximately on a flat bed).

In [5], a conformal map is given that transforms the flow domain $-\infty < x < \infty, -h_0 + h_b(x) \leqslant z \leqslant 0$ into a uniform strip $-\infty < \xi < \infty, -h \leqslant \eta \leqslant 0$ (see Fig. 2). The transformation functions are quoted here:

$$x = \xi - h\sum_{j=1}^{\infty}(b_j \sin 2j\xi - c_j \cos 2j\xi)\frac{\cosh 2j\eta}{\sinh 2jh}, \tag{9a}$$

$$z = \eta - h\sum_{j=1}^{\infty}(b_j \cos 2j\xi + c_j \sin 2j\xi)\frac{\sinh 2j\eta}{\sinh 2jh}. \tag{9b}$$

The depth h in the mapped plane and coefficients b_j and c_j are implicitly determined by

$$-h_0 + h_b(x) = -h + h\sum_{j=1}^{\infty}(b_j \cos 2j\xi + c_j \sin 2j\xi), \tag{10}$$

where

$$x = \xi - h\sum_{j=1}^{\infty}(b_j \sin 2j\xi - c_j \cos 2j\xi)\coth 2jh, \tag{11}$$

and subject to the condition

$$h + h^2\sum_{j=1}^{\infty} j\left(b_j^2 + c_j^2\right)\coth 2jh = h_0. \tag{12}$$

The map (9) preserves the intrinsic periodicity, since it is π periodic in both x and ξ. A method is given in [5], using a fast Fourier transform to compute the map parameters b_j, c_j, and h (hereafter collectively denoted by $\mathcal{B} = \{h, b_j, c_j, j = 1, 2, \ldots\}$). The Jacobian of the transformation is

$$J = x_\xi^2 + x_\eta^2. \tag{13}$$

Under the transformation, Eqs. (4)–(7) become

$$\phi_{\xi\xi} + \phi_{\eta\eta} = 0 \quad \text{for } -h < \eta < 0, \tag{14}$$

$$\phi_\eta = 0 \quad \text{at } \eta = -h, \tag{15}$$

$$\phi_{tt} + J^{-1/2}\phi_\eta - \kappa J^{-1/2}(J^{-1/2}(J^{-1/2}\phi_\eta)_\xi)_\xi = 0 \quad \text{at } \eta = 0. \tag{16}$$

In obtaining Eq. (16) we have combined the free-surface boundary conditions (6) and (7) and made use of $x_\eta = 0$ at $\eta = 0$. For a time-harmonic motion, $\phi = \varphi(\xi, \eta)e^{-i\sigma t} + \text{c.c.}$, where

$$\sigma = \omega/\sqrt{gk_B} \tag{17}$$

is the dimensionless frequency. The solution, which satisfies Eqs. (14) and (15), is of the Floquet type, i.e.,

$$\varphi(\xi, \eta) = e^{\mu\xi}P(\xi, \eta; \mu, \sigma), \tag{18}$$

where

$$P(\xi, \eta; \mu, \sigma) = \sum_{n=-\infty}^{\infty} D_n e^{in\xi}\frac{\cosh[(n - i\mu)(\eta + h)]}{\cosh[(n - i\mu)h]} \tag{19}$$

is the periodic factor for the Floquet exponent μ. By satisfying the free-surface boundary condition (16), we obtain the eigenvalue condition for μ, given a frequency σ, and the corresponding Fourier coefficients D_n in the eigenfunction (18). While the inclusion of surface tension does not change the general methodology, it does introduce some complexities in obtaining the eigenvalue condition due to the additional higher-order derivatives in Eq. (16). Defining

$$F(\xi) \equiv J^{1/2}|_{\eta=0} = 1 - h\sum_{j=1}^{\infty}(b_j \cos 2j\xi + c_j \sin 2j\xi)2j/\sinh 2jh, \tag{20}$$

we write, from Eq. (16),

$$-\sigma^2 F\varphi + \varphi_\eta - \kappa(G_3\varphi_{\eta\xi\xi} - G_2\varphi_{\eta\xi} - G_1\varphi_\eta) = 0 \quad \text{at } \eta = 0, \tag{21}$$

where

$$G_1 = -\tfrac{1}{2}(F^{-2})_{\xi\xi}, \quad G_2 = -\tfrac{3}{2}(F^{-2})_{\xi}, \quad G_3 = F^{-2}. \tag{22}$$

Since they are π periodic in ξ, without losing any generality, we can write

$$G_1 = \sum_{j=1,\infty} (g_{1j} e^{i2j\xi} + g_{1j}^* e^{-i2j\xi}), \tag{23}$$

$$G_2 = \sum_{j=1,\infty} (g_{2j} e^{i2j\xi} + g_{2j}^* e^{-i2j\xi}), \tag{24}$$

$$G_3 = g_{30} + \sum_{j=1,\infty} (g_{3j} e^{i2j\xi} + g_{3j}^* e^{-i2j\xi}), \tag{25}$$

where the asterisk stands for the complex conjugate and g_{30} is real. The Fourier coefficients g_{1j}, g_{2j}, and g_{3j} are functions of the map parameters $\mathcal{B}$ and hence known. Substituting Eqs. (18) and (23)–(25) into Eq. (21) and canceling the factor $e^{\mu\xi}$, we collect the coefficients of $e^{in\xi}$ and obtain

$$L_n D_n + \sum_{j=1,\infty} \Theta_{nj}^- D_{n-2j} + \Theta_{nj}^+ D_{n+2j} = 0, \tag{26}$$

where

$$L_n = -\sigma^2 + Z_n + \kappa[(n - i\mu)^2 g_{30}] Z_n, \tag{27}$$

$$\Theta_{nj}^- = \sigma^2 \frac{h(b_j - ic_j)j}{\sinh(2jh)} + \kappa[g_{1j} + i(n - 2j - i\mu)g_{2j} + (n - 2j - i\mu)^2 g_{3j}] Z_{n-2j}, \tag{28}$$

$$\Theta_{nj}^+ = \sigma^2 \frac{h(b_j + ic_j)j}{\sinh(2jh)} + \kappa[g_{1j}^* + i(n + 2j - i\mu)g_{2j}^* + (n + 2j - i\mu)^2 g_{3j}^*] Z_{n+2j}, \tag{29}$$

and

$$Z_n = (n - i\mu)\tanh[(n - i\mu)h]. \tag{30}$$

Now the recurrence relation (26) is formally the same as that in [5], except for the expressions of L_n and $\Theta_{nj}^{\pm}$. It is a homogeneous system $\mathsf{A}\bar{\mathsf{x}} = 0$, where A is an infinite square matrix and the column vector $\bar{\mathsf{x}}$ holds D_n. The expression of A is shown in [5] and omitted here for brevity. For nontrivial D_n, the determinant of A must vanish. This gives the eigenvalue condition for $\mu(\sigma)$, i.e., the dispersion relationship for linear waves, given the surface tension, the fluid depth, and a periodic bed profile. Defining $\Delta(\sigma, \mu; \kappa, h_0, \mathcal{B}) \equiv \det(\mathsf{A})$, we have

$$\Delta(\sigma, \mu; \kappa, h_0, \mathcal{B}) = 0. \tag{31}$$

The null vector of A gives D_n, which completes the eigenfunction (18) for the pair (μ and σ) that satisfies Eq. (31).

It can be seen from Eq. (26) that D_n for even and odd n do not couple since the coefficients in Eq. (21) are π periodic. Thus, the Fourier series in Eq. (19) can be represented using only odd or even n, corresponding to P being 2π or π periodic, respectively. A full Fourier series using all n is not necessary. This is the advantage of making the intrinsic periodicity be π. As is pointed out in Ref. [3], a solution represented with only odd n in Eq. (19) can be transformed into one with only even n, by replacing μ with $\mu + i$ or $\mu - i$, and vice versa. Even if we stick to a representation, say, with only odd n, by replacing μ with $\mu \pm 2i$ we should get different representations of the same kind. This artificial nonuniqueness can be suppressed by requiring that $-1 < \mathrm{Im}(\mu) \leqslant 1$.

Whereas either representation can be used for a solution, one is more convenient than the other, depending on the mode considered. This is tied in with the fact that μ is not arbitrary but must satisfy Eq. (31), which comes from the homogeneous system (26). By closely examining the asymptotic behaviors of the Floquet solutions at the limit when the bed becomes flat ($\Delta h_b \to 0$)

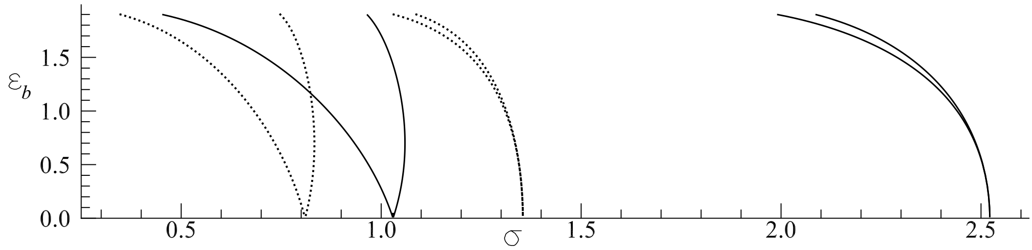

FIG. 3. First and second Bragg resonance tongues for a sinusoidal shape of bed profile for $h_0 = \pi/4$: ——, $\kappa = 0.6169$; $\cdots\cdots$, $\kappa = 0$.

and the properties of the infinite determinant, the previous studies [3–5] have provided a guideline that also applies here: For the wave modes, it is convenient to use an odd-n representation for the frequencies that are close to the odd m Bragg resonance bands (see Sec. III) and an even-n representation for those that are close to the even m resonance bands such that μ is pure imaginary or real corresponding to σ being outside or inside a band. Obviously, Bragg resonant wave modes (μ is real and small) cannot exist as free waves over an unbounded periodic bed, but must be considered in a finite domain where the lateral boundary conditions restrict the spatial decay (or growth) of the wave amplitude.

The focus of this study is on the wave modes which have spatially periodic flow fields, excluding Bragg resonant wave modes. The latter have been extensively studied during the development and in the applications of the exact Floquet theory [4–7]. To be used in Sec. IV, the waveform is given as follows. The surface elevation is $\zeta = \zeta_a(x)e^{-i\sigma t} + \text{c.c.}$, where

$$\zeta_a(x) = i\sigma^{-1}F^{-1}\sum_{n=-\infty}^{\infty} D_n e^{i(n-i\mu)\xi} Z_n, \tag{32}$$

following from the surface boundary condition (6), and

$$x = \xi - h\sum_{j=1}^{\infty}(b_j \sin 2j\xi - c_j \cos 2j\xi)/\sinh 2jh \tag{33}$$

at $z = 0$ ($\eta = 0$) according to the map (9).

III. BRAGG RESONANCE BANDS AND SPATIALLY PERIODIC MOTIONS

For gravity waves ($\kappa = 0$), Yu and Howard [5] have shown that on a periodic bed there are isolated narrow bands (or gaps) of frequencies for which μ is real. These are Bragg resonant frequencies, for which the eigenfunctions are standing waves with amplitudes varying exponentially (slowly) in space. Spatially periodic motions exist only for the frequencies outside a band where μ is pure imaginary or at the boundaries of a band where $\mu = 0$. This similarly occurs in the dispersion relationship (31) for capillary-gravity waves ($\kappa \neq 0$).

Define a relative undulation height $\epsilon_b = \Delta h_b/h_0$, where $\epsilon_b < 2$ to avoid the bed crests touching the free surface. This parameter may be used to measure the strength of nonuniformity of the medium. Given h_0 and the shape of the bed profile, the resonance bands form isolated tongues in the ϵ_b-σ plane. The boundaries of these tongues are the threshold frequencies $\sigma(\epsilon_b)$ for which $\mu = 0$. As ϵ_b increases, these tongues sweep towards low frequencies while the bandwidths increase, due to the decrease of effective depth h [5]; see Figs. 3–5 for selected bed profiles, where the cases of $\kappa = 0$ and $\kappa \neq 0$ are compared. Each resonance tongue emanates from the frequency of the flat-bottom wave whose wavelength $\lambda = (2/m)\lambda_b$, where $m = 1, 2, 3, \ldots$. The width of a band is wider compared to its counterpart for $\kappa = 0$, due to the greater downshift of the lower boundary

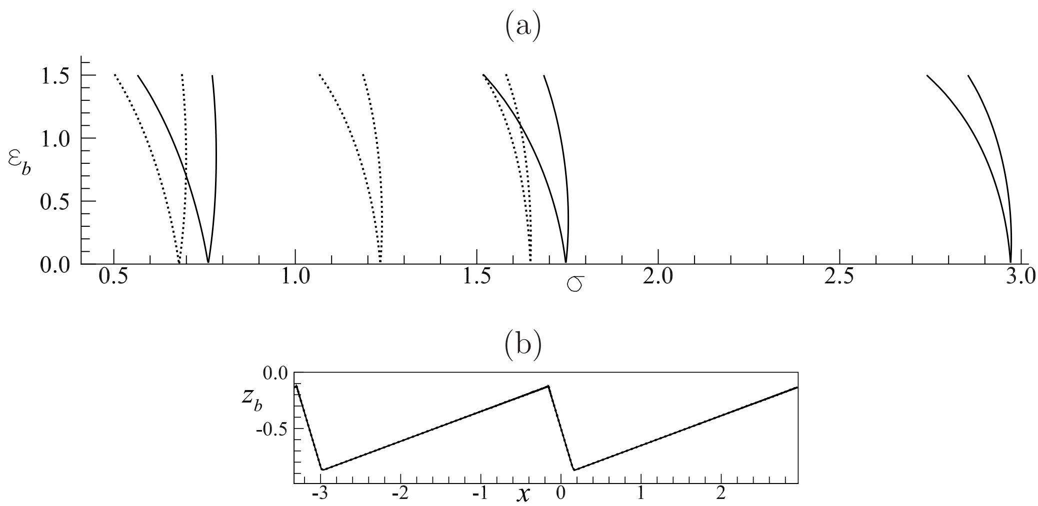

FIG. 4. (a) First, second, and third Bragg resonance tongues for a sawtooth shape of bed profile for $h_0 = 0.5$: ——, $\kappa = 0.25$; $\cdots\cdots$, $\kappa = 0$. (b) Bed profile for $\epsilon_b = 1.5$. The inversion of $\eta = -h$ is included (dotted curve) and indistinguishable from the solid curve, indicating the accuracy of the conformal map that is constructed.

of the tongue. For a sinusoidal bed profile, the $m > 1$ resonance tongues are extremely narrow. For other shapes, the bandwidths for $m > 1$ can be comparable to that of the primary band.

For a square-wave bed profile, the boundaries of the $m = 2$ resonance tongue transversally cross at $\epsilon_b \simeq 0.78$, leading to a pocket of unstable frequencies (cf. Fig. 5). This similarly occurs for the $m = 4$ resonance, but at a higher ϵ_b. (It is not shown here, but is shown for $\kappa = 0$ in [5].) As was discussed in Refs. [4,5], these Bragg resonance tongues bear some similar features to the unstable gaps for Mathieu's and Hill's equations, even though neither of the two equations directly appears in

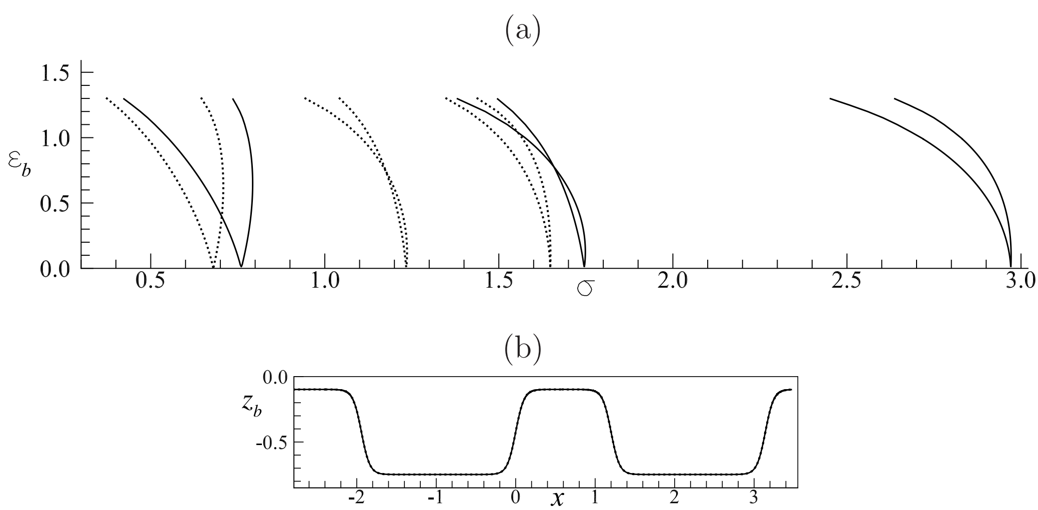

FIG. 5. (a) First, second, and third Bragg resonance tongues for a square-wave shape of bed for $h_0 = 0.5$: ——, $\kappa = 0.25$; $\cdots\cdots$, $\kappa = 0$. (b) Bed profile for $\epsilon_b = 1.3$. The inversion of $\eta = -h$ is shown as the dotted curve (indistinguishable).

the problem of water-wave Bragg resonances (except for the case of shallow water waves and small bed amplitude). For Hill's equation, transversal intersections of instability boundaries are known to occur when the periodic coefficient is a square wave (see, e.g., Ref. [14]).

IV. WAVEFORMS

For the frequencies outside a resonance band, $\mu = \pm i\nu$, $\nu > 0$, and the eigenfunctions give two oppositely propagating waves. For the threshold frequencies at the boundaries of a resonance band, $\mu = 0$ and the eigenfunctions give standing waves. These are the two kinds of spatially periodic motions that can exist as free waves over a periodic bed of indefinite length.

Since we will be dealing with spatially modulated linear waves, we must distinguish the wavelength of a wave and the spatial period of the flow under a wave. For a simple sinusoidal flat-bottom wave, the wavelength λ is defined as the horizontal distance between two consecutive corresponding points of a propagating waveform, say, two adjacent crests or troughs. The waveform identically repeats itself over one λ and so is the flow field under the wave. This is what we normally call a spatially periodic wave. Over a periodic bed, we may still define the wavelength λ as the horizontal distance between two adjacent wave crests (or troughs), even though the two crests may not be identical due to the spatial modulation. This wavelength λ cannot be directly deduced from $\mu = \pm i\nu$ in most cases, since it is determined by the eigenfunction, but λ usually is close to its flat-bottom counterpart for the same given frequency in the depth h_0. The spatial period of the flow field under the wave may be equal to or longer than λ, depending on the frequency. If the spatial period of the flow field is the same as the wavelength, the wave is spatially periodic, i.e., the waveform identically repeats itself over one λ. Otherwise, the wave is spatially modulated.

The standing waves for $\mu = 0$ may also be spatially modulated, again depending on the frequency (see Sec. IV B). It should be emphasized that these standing waves are not the superposition of two oppositely directed waves as in the flat-bottom case. For these threshold frequencies at the boundaries that separate the spatially periodic and nonperiodic motions, linear waves can only exist in the form of standing waves due to the scattering by topography.

To avoid confusion in the discussion that follows, it should also be mentioned that there are multiple frequencies σ that satisfy Eq. (31) for a given μ (see the Appendix). The eigenfunction (18), however, is uniquely determined, since the null vectors are distinct for individual pairs (σ, μ). This in fact is seen in the case of $\mu = 0$. The nonunique correspondence between μ and σ is well known in the study of Bloch waves in solids which are given in Floquet forms.

A. Propagating waves: $\mu = \pm i\nu$

Over a periodic bed, spatially periodic propagating waves, in the sense that the waveform identically repeats itself over one wavelength, can only occur when $\lambda = m\lambda_b$ and the integer $m > 2$. Otherwise, the two adjacent wave crests (or troughs) are not identical, since they are situated above the different parts of the bed profile at any given time, and the wave must modulate in space. The modulation period is $2\pi/(1-\nu)$. These may also be called quasispatially periodic waves, as the waveform nearly repeats over one λ. In this study, the quasispatially periodic waves and spatially modulated waves are interchangeable. Clearly, high-frequency waves of $\lambda < \lambda_b$ always modulate in space.

The waveforms at different phases of a wave cycle are shown in Fig. 6 for a sinusoidal bed, comparing the cases of gravity ($\kappa = 0$) and capillary-gravity wave ($\kappa \neq 0$). In both cases, we choose a spatially periodic wave of $\lambda = 3\pi$ ($\mu = -i\frac{1}{3}$) and a quasispatially periodic wave of $\lambda = 1.5\pi$ ($\mu = i\frac{1}{3}$) that modulates over a spatial period of 3π. The sign of μ is chosen for the propagation in the $+x$ direction. Recall that the dimensionless bed period is π. For both classes of gravity and capillary-gravity waves, the waveforms are not permanent: As the wave propagates, the relative position between the surface waveform and the bed profile changes. Consequently, the waveform must continuously changes its shape over a wave cycle. The instantaneous waveform can

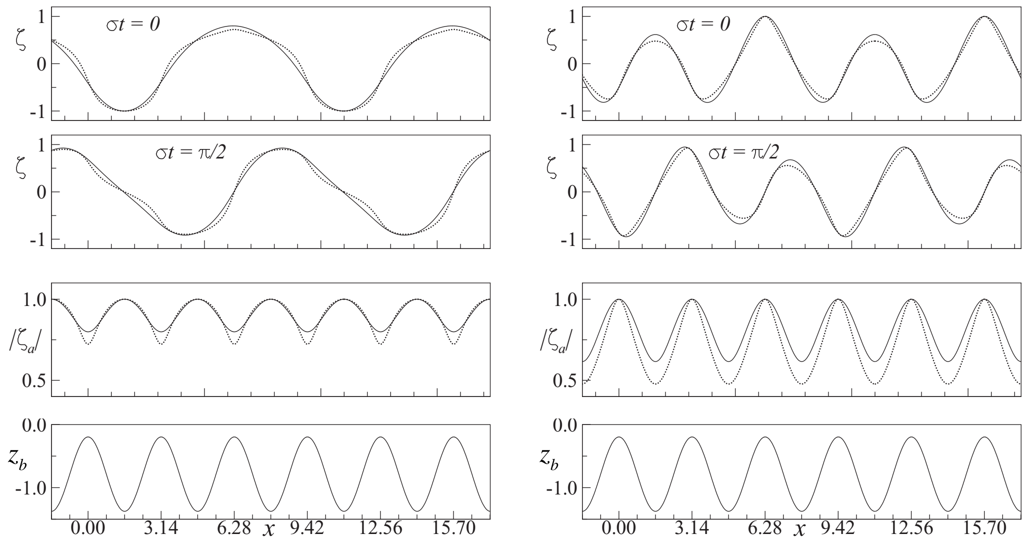

FIG. 6. Propagating waveforms at different times of a wave cycle and oscillation amplitude $|\zeta_a|$ on a sinusoidal bed of height $\epsilon_b = 1.5$ for $h_0 = \pi/4$. On the left is a spatially periodic wave of $\lambda = 3\pi$ ($\mu = -i\frac{1}{3}$): ——, $\sigma = 0.4930$ for $\kappa = 0.6169$; $\cdots\cdots$, $\sigma = 0.4314$ for $\kappa = 0$. On the right is a spatially modulated wave of $\lambda = 1.5\pi$ ($\mu = i\frac{1}{3}$): ——, $\sigma = 1.3118$ for $\kappa = 0.6169$; $\cdots\cdots$, $\sigma = 0.9111$ for $\kappa = 0$. The bed profile z_b is included for easy identification of the relative locations of surface wave crests and troughs, $|\zeta_a|_{\max}$ and $|\zeta_a|_{\min}$, with respect to the bed crest and trough; see the text in Sec. IV A.

be asymmetric with respect to the wave crest (or trough), even though the bed profile is perfectly left-right symmetric; see Fig. 6 at $\sigma t = \pi/2$. The surface wave patterns in space-time are illustrated in Fig. 7. The oscillation amplitude $|\zeta_a|$ varies at the scale of bed period π, regardless of the surface wavelength (cf. Fig. 6), and is symmetric in x, following the symmetry of topography. The variability in $|\zeta_a|$ is greater for the wave of $\lambda = 1.5\pi$, indicating stronger wave scattering by topography when the frequency is closer to the primary Bragg resonance band. The spatial periodicity of $|\zeta_a|$ distinguishes these waves from the partially reflected flat-bottom waves. In the latter case, the oscillation intensity varies over one half the surface wavelength, manifested by the spacing of surface envelope maxima (or minima).

For capillary-gravity waves, the waveform geometry depends also on the surface tension κ. This is in contrast to the flat-bottom case where surface tension only modifies the dispersion relationship and does not affect the geometry of linear waveforms. Given a wavelength, the waveform for $\kappa \neq 0$ is noticeably smoother than that for $\kappa = 0$. The variability in $|\zeta_a|$ is reduced with $\kappa \neq 0$, suggesting that the capillary effect tends to counteract the effect of higher harmonic generation in wave-topography interaction. On an asymmetric bed profile, the effect of surface tension tends to reduce the spatial asymmetry in the waveform; see Fig. 8 for propagating waves over a nonsmooth bed profile.

B. Standing waves: $\mu = 0$

Given a bed undulation height ϵ_b and mean depth h_0, there are two threshold frequencies at the boundaries of the mth band. Correspondingly, there are two independent standing waves, both having the same wavelength $\lambda = 2\lambda_b/m$. Although the frequencies are fairly close because of the narrow bandwidth, the two standing waves have drastically different waveforms (eigenfunctions). For $m = 1, 2$, $\lambda = 2\lambda_b$ and $\lambda = \lambda_b$, respectively, and the standing waves are spatially periodic, i.e., the two adjacent waveforms are identical. For $m > 2$, they are quasispatially periodic standing

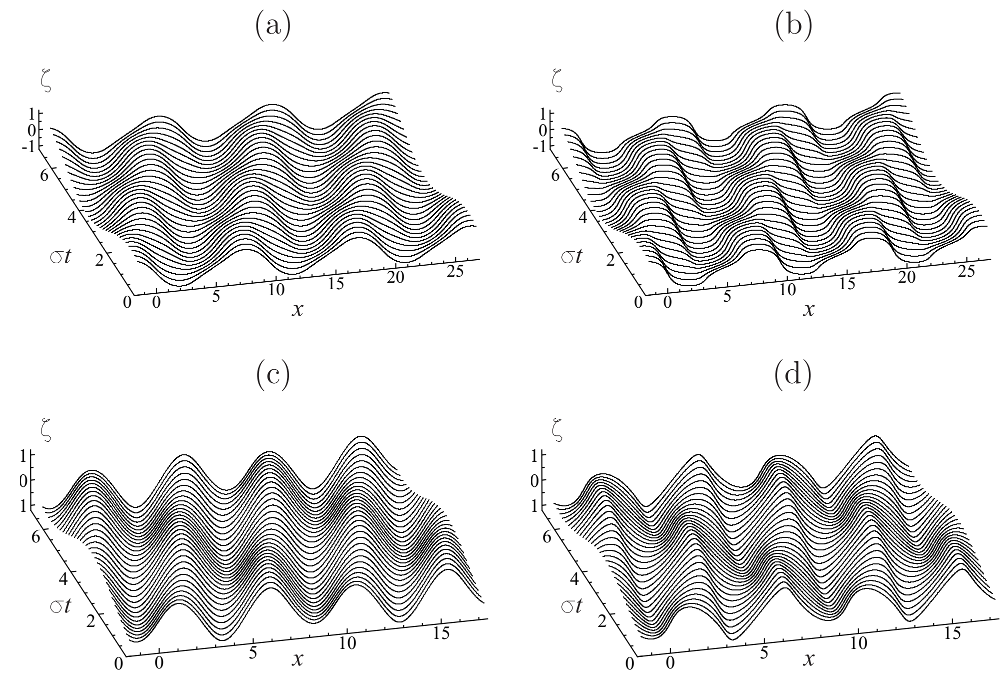

FIG. 7. Surface wave patterns in space-time of the propagating waves in Fig. 6, for $\lambda = 3\pi$ in (a) $\kappa = 0.6169$ and (b) $\kappa = 0$ and for $\lambda = 1.5\pi$ in (c) $\kappa = 0.6169$ and (d) $\kappa = 0$.

waves since $\lambda < \lambda_b$. The modulation period of the standing waves is $2\lambda_b$ for odd m or λ_b for even m. Examples are given in Fig. 9 for a sinusoidal bed and in Fig. 10 for a square-wave bed profile.

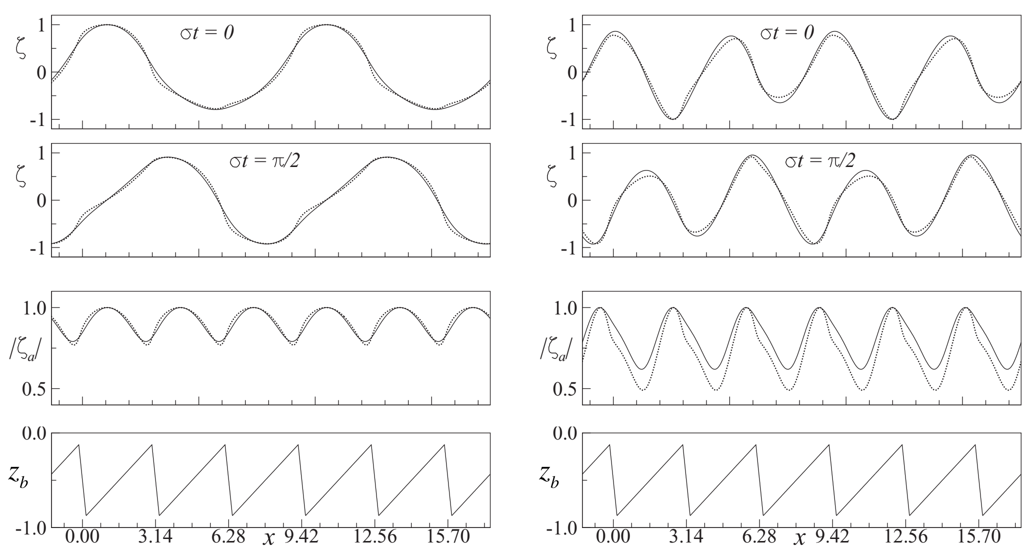

FIG. 8. Propagating waveforms at different times of a wave cycle and oscillation amplitude $|\zeta_a|$ on a sawtooth bed of $\epsilon_b = 1.5$ for $h_0 = 0.5$. On the left is a spatially periodic wave of $\lambda = 3\pi$ ($\mu = -i\frac{1}{3}$): ——, $\sigma = 0.4063$ for $\kappa = 0.25$; $\cdots\cdots$, $\sigma = 0.3830$ for $\kappa = 0$. On the right is a spatially modulated wave of $\lambda = 1.5\pi$ ($\mu = i\frac{1}{3}$): ——, $\sigma = 0.9611$ for $\kappa = 0.25$; $\cdots\cdots$, $\sigma = 0.7992$ for $\kappa = 0$.

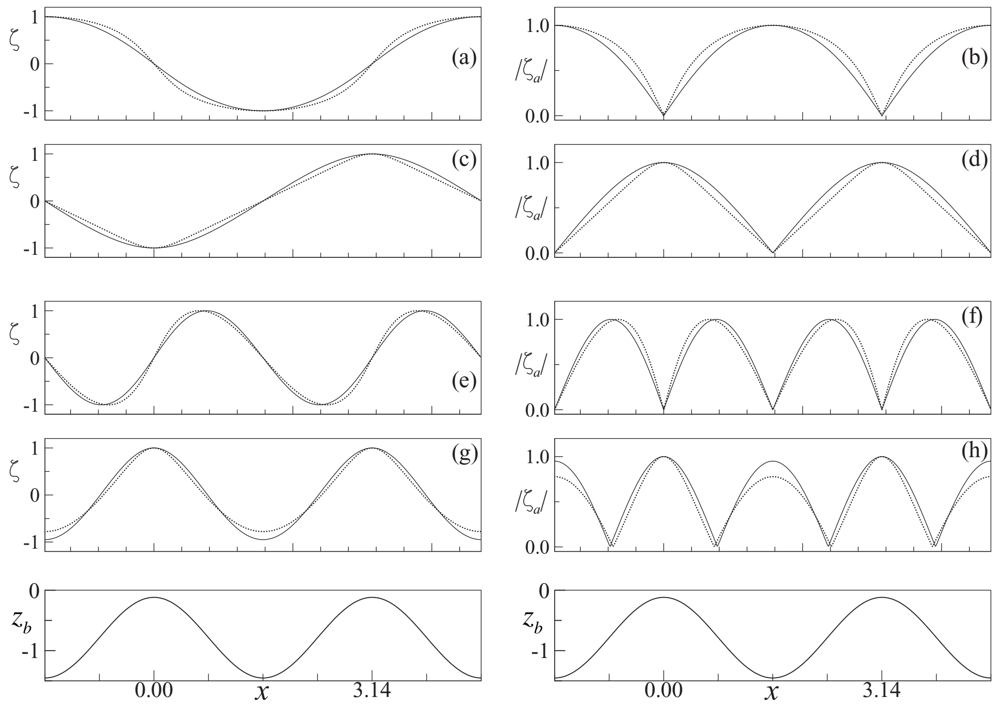

FIG. 9. Shown on the left are instantaneous surface waveforms and on the right oscillation amplitudes $|\zeta_a|$ of standing waves for the threshold frequencies of the mth resonance band on a sinusoidal bed of $\epsilon_b = 1.5$ for $h_0 = \pi/4$. The instance is when the oscillations at antinodes reach the maximum. The case for $\kappa = 0$ is shown in dotted curves. For $m = 1$, (a) and (b) $\sigma = 0.7089$ for $\kappa = 0.6169$ and $\sigma = 0.5550$ for $\kappa = 0$ and (c) and (d) $\sigma = 1.0236$ for $\kappa = 0.6169$ and $\sigma = 0.8027$ for $\kappa = 0$. For $m = 2$, (e) and (f) $\sigma = 2.2898$ for $\kappa = 0.6169$ and $\sigma = 1.2246$ for $\kappa = 0$ and (g) and (h) $\sigma = 2.3199$ for $\kappa = 0.6169$ and $\sigma = 1.2415$ for $\kappa = 0$. The bed profile is included for easy identification of the relative locations of the surface wave crests and troughs (left column) and surface antinodes and nodes (right column), with respect to the bed crest and trough; see the text in Sec. IV B.

For $m = 1$, the surface antinodes (or nodes) are λ_b apart. For the lower threshold frequency, the antinodes and nodes are, respectively, above the bed troughs and crests. This leads to a surface waveform with a broad wave crest [cf. Figs. 9(a) and 10(a)]. For the higher threshold frequency, the antinodes are at the bed crests. Consequently, the surface waveform has a sharp wave crest due to the shallow water depth under the antinode [cf. Figs. 9(c) and 10(c)]. For gravity waves, the wave crests can become protuberant when the bed crests are sufficiently high [cf. Fig. 10(c)]. The surface tension reduces the geometric extreme in the waveform, tending to restore the sinusoidal form. For time-harmonic motions, the phase of oscillation at a give location reverses every half wave cycle in time. The standing oscillations at two adjacent antinodes are completely out of phase. Thus, a broad wave crest becomes a broad wave trough (for the lower frequency) and a sharp crest becomes a sharp trough (for the higher frequency), at every half wave cycle.

For $m = 2$, the surface antinodes (or nodes) are $\lambda_b/2$ apart. For the lower threshold frequency, the antinodes are above the slopes between the bed crests and troughs, while the locations of nodes alternate between the bed crests and troughs. This renders the waveform nonsymmetric in x even though the bed profile is symmetric. This is particularly noticeable for gravity waves [cf. Fig. 9(e)]. For the higher threshold frequency, the waveform is symmetric since the locations of surface antinodes alternate between the bed crests and troughs. Thus, at an instance the waveform appears to have a sharp wave crest over the bed crest followed by a broad wave trough over the

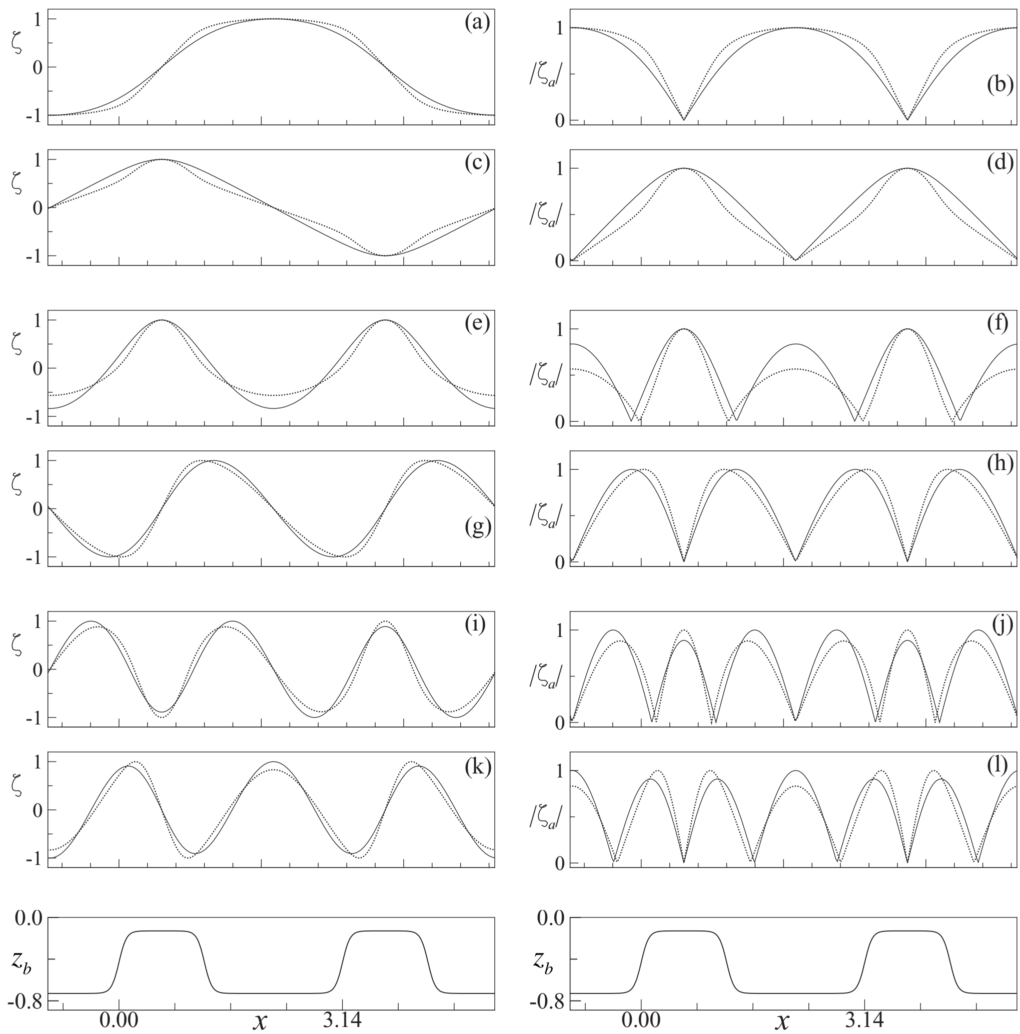

FIG. 10. Shown on the left are instantaneous surface waveforms and on the right oscillation amplitudes $|\zeta_a|$ of standing waves for the threshold frequencies of the mth resonance bands on a square-wave bed of $\epsilon_b = 1.2$ for $h_0 = 0.5$. The instance is when the oscillations at antinodes reach the maximum. The case for $\kappa = 0$ is shown in dotted curves. For $m = 1$, (a) and (b) $\sigma = 0.4701$ for $\kappa = 0.25$ and $\sigma = 0.4182$ for $\kappa = 0$ and (c) and (d) $\sigma = 0.7558$ for $\kappa = 0.25$ and $\sigma = 0.6686$ for $\kappa = 0$. For $m = 2$, (e) and (f) $\sigma = 1.4607$ for $\kappa = 0.25$ and $\sigma = 1.0114$ for $\kappa = 0$ and (g) and (h) $\sigma = 1.5396$ for $\kappa = 0.25$ and $\sigma = 1.0796$ for $\kappa = 0$. For $m = 3$, (i) and (j) $\sigma = 2.5592$ for $\kappa = 0.25$ and $\sigma = 1.4133$ for $\kappa = 0$ and (k) and (l) $\sigma = 2.7172$ for $\kappa = 0.25$ and $\sigma = 1.4962$ for $\kappa = 0$.

bed trough [cf. Fig. 9(g)]; a half wave cycle later, a sharp wave trough will appear at the bed crest followed by a broad wave crest at the bed trough. The oscillation amplitude is greater over the bed crests [cf. Fig. 9(h)]. The effect of surface tension considerably increases $|\zeta_a|$ at the bed trough, tending to render the waveform spatially sinusoidal. In the case when the boundaries of a resonance tongue transversely cross, the properties of the waveform stay with the respective boundaries. For example, for the square-wave profile, the $m = 2$ resonance tongue has a transversal crossing at $\epsilon_b = 0.78$ (cf. Fig. 5). The asymmetric and symmetric waveforms are affiliated, respectively, with

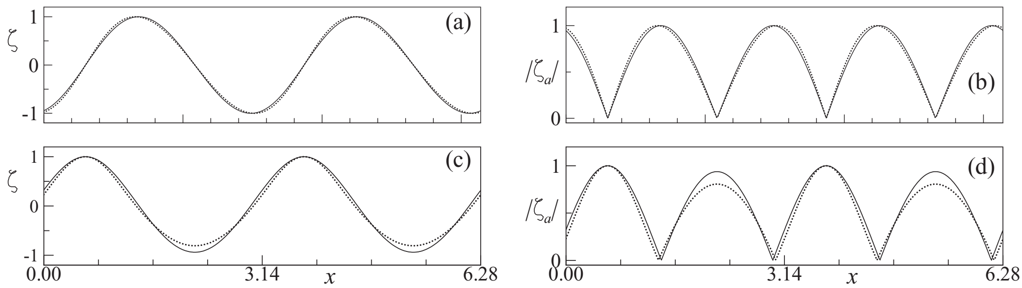

FIG. 11. Instantaneous surface waveforms and oscillation amplitudes $|\zeta_a|$ of standing waves for the threshold frequencies of the $m = 2$ resonance band on a square-wave bed of $\epsilon_b = 0.7$, showing the affiliations of waveform with the appropriate boundaries before the transverse crossing of instability boundaries occurs (comparing with that for $\epsilon_b = 1.2$ after the crossing in Fig. 10). The case for $\kappa = 0$ is shown in dotted curves. (a) and (b) $\sigma = 1.6721$ for $\kappa = 0.25$ and $\sigma = 1.1812$ for $\kappa = 0$ and (c) and (d) $\sigma = 1.6792$ for $\kappa = 0.25$ and $\sigma = 1.1842$ for $\kappa = 0$.

the lower and higher threshold frequencies for $\epsilon_b < 0.78$, but with the higher and lower frequencies for $\epsilon_b > 0.78$ [cf. Fig. 11 and Figs. 10(e)–10(h)].

For $m > 2$, $\lambda < \lambda_b$ and the spacing between two adjacent surface antinodes (or nodes) is less than $\lambda_b/2$. As a result, the antinodes can be above the bed crests, the bed troughs, ad the slopes in between. Consequently, there is a mixture of asymmetric and symmetric standing waveforms within a modulation period; see Figs. 10(i)–10(l) for $m = 3$.

C. Reminiscences of nonlinear waveforms

Modulations and asymmetry of waveform would have arisen from nonlinear effects for waves on a flat bed, but occur for linear waves over a periodic bed. For the linear standing wave over a bed of large undulation height [cf. Fig. 10(c)], the geometry of the protuberant wave crests bears striking resemblance to that of highly nonlinear standing waves in deep water [15]. The high curvature in the waveform geometry manifests higher-order spatial harmonics. These observed reminiscences of nonlinear waveforms are intriguing and not coincident.

The apparent similarities are related to the generation of spatial harmonics, hence spatial nonuniformity in oscillations, which mathematically traces back to quadratic interactions between waves. For two-dimensional nonlinear wave motions, the quadratic products $\phi_x\zeta_x$ and $|\nabla\phi|^2$ in the free-surface boundary conditions generate time harmonics and simultaneously spatial harmonics. This makes the oscillation amplitude nonuniform in space and time, causing the nonlinear waveform to be spatially and temporally nonsinusoidal, hence modulating in space-time, or even becoming unstable. As the oscillation becomes temporally nonsinusoidal, the wave crest and tough (corresponding to the two opposite extreme phases of a time cycle) are no longer the mirror reflections of each other as in the case of linear waves. For the nonlinear standing waves in Ref. [15], the wave troughs are flat while the wave crests are protuberant. On a periodic bed, the interaction of the wave and bed is manifested by the quadratic product $J^{-1/2}\phi_\eta$ and its derivatives in the free-surface boundary condition (16), where the Jacobian of transformation J represents the bed. If we regard the periodic bed as a wave of zero frequency, wave-bottom interaction is mathematically a special case of quadratic wave-wave interaction that generates only spatial harmonics but not time harmonics. Thus, the waveform is spatially nonsinusoidal and modulates as it propagates in responding to the spatially nonuniform oscillations. The dynamics of the flow still is linear due to the inability to generate time harmonics by wave-bottom interaction. For time-harmonic motions, the wave crest and trough thus remain mirror reflections of each other, despite the spatial complexity of the waveform. This of course will be changed when the nonlinearity takes effect. Whereas there seems to be a mathematical basis for some similarities in the waveforms, this does not suggest any analogy between the physics of wave-bottom interaction and that of nonlinear wave-wave interaction, especially not from a dynamical point of view.

V. CONCLUSION

We have given an extensive examination of the waveforms of linear waves over a periodic bed, using the exact Floquet theory for gravity waves in [5] and its extension to capillary-gravity waves developed in this study. For these waves, the waveform geometry is frequency dependent and affected by surface tension, having complex features that cannot be anticipated based on the knowledge of ordinary linear harmonics waves. For the frequencies outside a Bragg resonance band, the propagating waves can be spatially periodic or spatially modulating, depending on whether or not the surface wavelength is an integer ($m > 2$) multiple of the bed period. In both cases, the waveform geometry changes in time over a wave cycle, as the wave propagates. The instantaneous waveform can be left-right asymmetric with respect to the wave crest (or trough) even though the topography is symmetric. Of particular interest are the standing waves for the threshold frequencies at the boundaries of the mth Bragg resonance band. For each m, two independent standing waves can be found, having the same wavelength $2\lambda_b/m$ but slightly different frequencies. Their waveforms (eigenfunctions) are drastically different, e.g., one is left-right symmetric with respect to the wave crest (or trough) and the other is not, even though they are on the same symmetric topography. The standing waves can have high-curvature wave-crest forms that resemble the nonlinear standing waveforms in deep waters. For both propagating and standing waves, the effect of surface tension is seen to counteract wave scattering by topography, tending to reduce the geometric extremes and asymmetry in the waveforms.

The results presented here are fundamental to linear waves over a variable (periodic) bed, since they are based on the eigenmodes of the system, not from the solution of a particular problem or application. We expect that the understanding of these general solutions will inspire new applications and open scientific questions for further studies. For instance, are the standing waves at the threshold frequencies of a resonance band both stable? Considering that their frequencies are so close and yet their waveforms are so different, does one standing wave tend to be more stable to perturbations than the other? Can they be sufficiently stable to be observed?

By definition, linear waves are of infinitesimal amplitude. The exact Floquet solutions therefore will breakdown when surface nonlinearity kicks in. This can particularly be an issue when the oscillation intensity becomes strongly nonuniform in space due to topographic scattering and causes the waveform to locally develop high curvatures. Since the linear waveforms are already frequency dependent, one may expect that these waves are more susceptive to frequency perturbations in the subsequent nonlinear wave propagation, compared to their flat-bottom counterparts. Nachbin [16] and most recently Fokas and Nachbin [17] studied weakly nonlinear shallow water waves interacting with variable topographies, using a numerical conformal transformation of Schwarz-Christoffel type. In those studies, the flat-bottom dispersion relationship and linear sinusoidal wave were assumed (or implied). In the presence of a bed topography, the frequency for a given surface wavelength is downshifted and the linear waveforms can significantly deviate from their flat-bottom counterparts in a number of aspects, as we have seen in this study. It is interesting to see how the exact Floquet theory of linear water waves can be incorporated into some existing methods of nonlinear analyses.

For future research, some improvements and applications are worth mentioning. (i) Some physical phenomena examined here are expected to similarly occur in the interfacial waves in layered fluids over a periodic bed. This can be studied using the exact theory of Yu and Maas [18]. (ii) In practical applications, the effects of viscosity can be important. For gravity waves, Yu [19] presented a terrain-following wave boundary layer model. This can be adapted to study the Stokes boundary layers under capillary-gravity waves, combined with the solutions in this paper.

(iii) Some applied problems are interesting, e.g., resonant standing waves on the surface of a fluid in a vibrating tank or container with a corrugated bottom, considering one- and two-layer fluid, and the effects of surface tension.

ACKNOWLEDGMENTS

Part of the material in this study was developed when the author was supported by U.S. National Science Foundation (Grant No. CBET-0845957). The author wishes to thank an anonymous reviewer whose comments have helped to improve the paper. The author is particularly grateful to Professor Leo R. M. Maas.

APPENDIX: CALCULATIONS OF THE DISPERSION RELATIONSHIP (31)

For brevity, we will use the notation $\Delta(\sigma, \mu)$, suppressing the dependence on κ, h_0, and $\mathcal{B}$. For $\kappa = 0$, Yu and Howard [5] have proven that $\Delta(\sigma, \mu)$ is real for pure imaginary or real μ, based on the symmetry properties of A. For the case $\kappa \neq 0$, some of the symmetry properties are lost, since Θ_{nj}^{+} and Θ_{nj}^{-} are no longer complex conjugates [cf. Eqs. (28) and (29)]. However, the calculations show that $\Delta(\sigma, \mu)$ is real (or can be scaled to be so) when the periodic factor (19) is represented using the appropriate odd- or even-n representation (cf. Sec. II). The convergence of the infinite determinant was discussed in [5]. This similarly holds for $\kappa \neq 0$. Since multiplying the rows by suitable (positive) factors will not affect the roots of Eq. (31), one can improve the condition number of A by appropriate normalization.

The function $\Delta(\sigma, \mu)$ can readily be computed, e.g., using MATLAB, hence finding the roots of Eq. (31). We will first consider the limiting case of a flat bed ($\Delta h_b = 0$) for the purpose of verification. When $\Delta h_b = 0$, $\xi = x$, $\eta = z$, and $h = h_0$. The Floquet solution (18) should reduce to the simple sinusoidal waves and Eq. (31) should give the same frequency–wave-number relation as described by the flat-bottom dispersion relationship (see Sec. I), which upon using the normalization

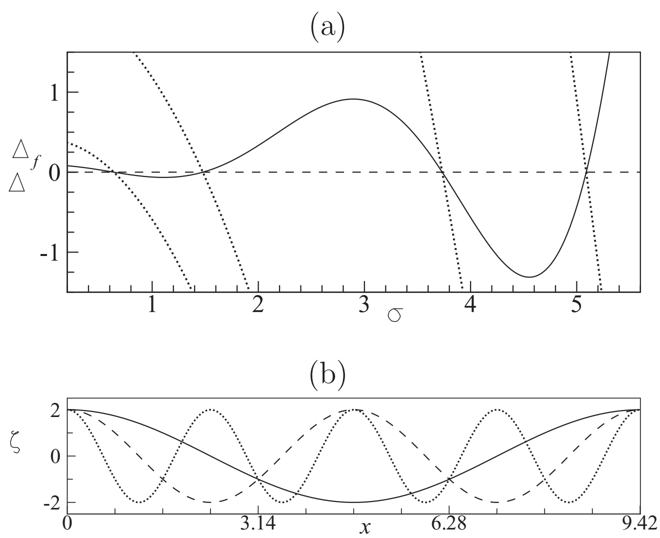

FIG. 12. (a) Plot of $\Delta(\sigma, \mu)$ with $\mu = i\frac{1}{3}$ for a flat bed ($\Delta h_b = 0$): ——, Re(Δ); – – –, Im(Δ). Dotted curves are $\Delta_f(\sigma)$ for $k/k_B = 2/3$, $4/3$, $8/3$, and $10/3$. (b) Waveforms at $t = 0$ calculated using Eq. (32) for the first three roots in (a): ——, $\sigma = 0.6368$ ($\lambda = 3\pi$); – – –, $\sigma = 1.4773$ ($\lambda = 3\pi/2$); $\cdots\cdots$, $\sigma = 5.0894$ ($\lambda = 3\pi/4$), for $h_0 = \pi/4$ and $\kappa = 0.6169$.

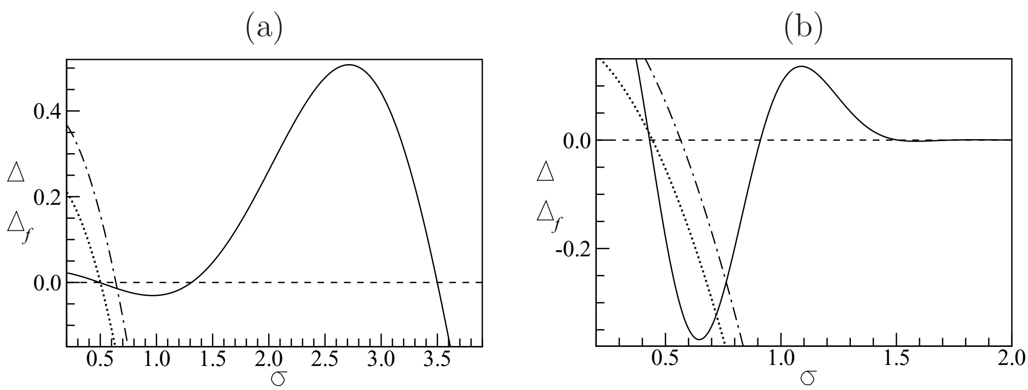

FIG. 13. (a) Plot of $\Delta(\sigma, \mu)$ with $\mu = i\frac{1}{3}$ for a bed profile $h_b/h_0 = \frac{3}{4}\cos(2x)$ and $h_0 = \pi/4$, showing the first three roots, with ——, Re(Δ) and − − −, Im(Δ), and plot of $\Delta_f(\sigma)$ for $k/k_B = 2/3$, with - · - · -, using $h_0 = \pi/4$, and $\cdots\cdots$, using the depth $h = 0.4571$ in the mapped plane for $\kappa = 0.6169$. (b) Corresponding graph of $\Delta(\sigma)$ and $\Delta_f(\sigma)$ with $\kappa = 0$.

in Eq. (3) is written as

$$\Delta_f(\sigma, \mu_f) \equiv \mu_f \tanh(\mu_f h_0)\big(1 + \kappa\mu_f^2\big) - \sigma^2 = 0, \tag{A1}$$

where $\mu_f = k/k_B$.

For $\mu = \pm i\nu$, $\nu > 0$, the spatial period of the Floquet solution is $2\pi/(1-\nu)$. Since wavelengths $(1/m)2\pi/(1-\nu)$, $m = 1, 2, 3, \ldots$, can all fit into this spatial period, there are multiple frequencies σ that satisfy Eq. (31) for a given μ, corresponding to wave numbers $k/k_B = m(1-\nu)$. In Fig. 12(a), $\Delta(\sigma, \mu)$ is plotted for $\Delta h_b = 0$, showing the first four roots $\sigma = 0.6389, 1.4773, 3.7329, 5.0894$ for $\mu = i\frac{1}{3}$. These are the frequencies for wave numbers $k/k_B = \frac{2}{3}, 2(\frac{2}{3}), 4(\frac{2}{3}), 5(\frac{2}{3})$, i.e., wavelengths $3\pi, \frac{3}{2}\pi, \frac{3}{4}\pi, \frac{3}{5}\pi$. These results are confirmed by the graphs of $\Delta_f(\sigma, \mu_f)$ in Fig. 12(a). For each pair of (σ, μ), the state of motion is unique and given by the eigenfunction (18). The waveform ζ is computed using Eq. (32) for the first three frequencies and seen to be precisely sinusoidal in x with the anticipated wavelengths [see Fig. 12(b)]. Note that the frequency for $\lambda = \pi$, i.e., $k/k_B = 3(\frac{2}{3})$, is missing in Fig. 12(a) but can be recovered using an even-n representation where P is π periodic.

Keeping the mean fluid depth h_0 and surface tension parameter κ the same as in Fig. 12, the graph of $\Delta(\sigma, \mu)$ for a sinusoidal bed profile is plotted in Fig. 13(a), showing the roots $\sigma = 0.4930, 1.3118, 3.4990, \ldots$ for $\mu = i\frac{1}{3}$. The lowest frequency corresponds to the wave of wavelength 3π, while the higher ones are for the shorter waves that modulate over the spatial period of 3π. Comparing with the above values of σ for $\Delta h_b = 0$, the presence of a bed topography causes the frequency of motion to downshift for a given wavelength. Since the surface waves are more affected by the bed crests and less so by the bed troughs that are deeper, the depth that characterizes the propagation of waves is less than the mean depth h_0, being effectively given by the depth h in the mapped plane [5]. This explains the downshift of frequency. For the sinusoidal bed in Fig. 13, $h = 0.4571$ for $h_0 = \pi/4$. In fact, using h in the flat-bottom dispersion relationship above, one can obtain an estimate of the frequency for the periodic wave of $\lambda = 3\pi$, fairly close to the result given by Eq. (31) [cf. Fig. 13(a)]. This quick estimate becomes less accurate for spatially modulated waves (see Sec. IV A).

To fix the idea, suppose we consider a thin layer of water over a sinusoidal bed. The parameters in Fig. 13(a) can be obtained based the physical values: the mean depth $h_0' = 2.73$ mm, the bed period $\lambda_b = 10.90$ mm, and undulation height $\Delta h_b' = 1.5h_0'$ mm, compared with the critical wavelength $\lambda_c = 17.12$ mm.

[1] C. C. Mei, *The Applied Dynamics of Ocean Surface Waves* (World Scientific, Singapore, 1989).
[2] G. A. Athanassoulis and K. A. Belibassakis, A consistent coupled-mode theory for the propagation of small-amplitude water waves over variable bathymetry regions, J. Fluid Mech. **389**, 275 (1999).
[3] L. N. Howard and J. Yu, Normal modes of a rectangular tank with corrugated bottom, J. Fluid Mech. **593**, 209 (2007).
[4] J. Yu and L. N. Howard, On higher order Bragg resonance of water waves by bottom corrugations, J. Fluid Mech. **659**, 484 (2010).
[5] J. Yu and L. N. Howard, Exact Floquet theory for waves over arbitrary periodic topographies, J. Fluid Mech. **712**, 451 (2012).
[6] J. Yu and G. Zheng, Exact solutions for wave propagation over a patch of large bottom corrugations, J. Fluid Mech. **713**, 362 (2012).
[7] P. D. Weidman, A. Herczynski, J. Yu, and L. N. Howard, Experiments on standing waves in a rectangular tank with a corrugated bed, J. Fluid Mech. **777**, 122 (2015).
[8] H. Lamb, *Hydrodynamics* (Cambridge University Press, Cambridge, 1932).
[9] F. Dias and C. Kharif, Nonlinear gravity and capillary-gravity waves, Annu. Rev. Fluid Mech. **31**, 301 (1999).
[10] M. Perlin and W. W. Schultz, Capillary effects on surface waves, Annu. Rev. Fluid Mech. **32**, 241 (2000).
[11] R. Barakat and A. Houston, Nonlinear periodic capillary-gravity waves on a fluid of finite depth, J. Geophys Res. **73**, 6545 (1968).
[12] D. Henry, Particle trajectories in linear periodic capillary and capillary-gravity water waves, Philos. Trans. R. Soc. A **365**, 2241 (2007).
[13] H.-C. Hsu, M. Francius, P. Montalvo, and C. Kharif, Gravity-capillary waves in finite depth on flows of constant vorticity, Proc. R. Soc. A **472**, 20160363 (2016).
[14] H. Broer and M. Levi, Geometrical aspects of stability theory for Hill's equations, Arch. Rat. Mech. Anal. **131**, 225 (1995).
[15] W. W. Schultz, J.-M. Vanden-Broeck, L. Jiang, and M. Perlin, Highly nonlinear standing water waves with small capillary effect, J. Fluid Mech. **369**, 253 (1998).
[16] A. Nachbin, The localization length of randomly scattered water waves, J. Fluid Mech. **296**, 353 (1995).
[17] A. S. Fokas and A. Nachbin, Water waves over a variable bottom: A non-local formulation and conformal mappings, J. Fluid Mech. **695**, 288 (2012).
[18] J. Yu and L. R. M. Maas, Linear waves in two-layer fluids over periodic bottoms, J. Fluid Mech. **794**, 700 (2016).
[19] J. Yu, A terrain-following model of wave boundary layers, Ocean Model. **108**, 20 (2016).